Title
THE TERBIUM-IRON PHASE DIAGRAM

Author
Dariel, M.P.

Publication Date
1975-06-01

Submitted to Journal of the Less-Common Metals

LBL-3928
Preprint c.1

THE TERBIUM-IRON PHASE DIAGRAM

M. P. Dariel, J. T. Holthuis, and M. R. Pickus

June 1975

Prepared for the U. S. Energy Research and Development Administration under Contract W-7405-ENG-48

DISCLAIMER

THE TERBIUM-IRON PHASE DIAGRAM

M. P. Dariel,* J. T. Holthuis and M. R. Pickus

Inorganic Materials Research Division, Lawrence Berkeley Laboratory and Department of Materials Science and Engineering, College of Engineering; University of California, Berkeley, California 94720

Summary

The terbium-iron phase diagram has been determined using metallographic, X-ray diffraction, differential thermal analysis, and electron microprobe techniques. The terminal solubilities of the two elements are extremely restricted, of the order of 0.1 at.% for Tb in Fe. A eutectic reaction takes place at 28 at.% Fe, 847°C. The four intermetallic compounds, $TbFe_2$, $TbFe_3$, Tb_6Fe_{23}, and Tb_2Fe_{17} melt non-congruently at 1187, 1212, 1276, and 1312°C respectively. The Tb_2Fe_{17} compound appears in the rhombohedral Th_2Zn_{17} modification on the Tb-rich side and the hexagonal Th_2Ni_{17} modification on the Fe-rich side of the stoichiometric composition.

* At leave from the Department of Material Engineering, Ben-Gurion University of the Negev, Beer-Sheva and the Nuclear Research Center Negev.

Introduction

The equilibrium phase diagrams of most rare-earth metal-iron binary systems have been reported in the literature.[1-7] Notable exceptions are the bivalent rare-earth metals Eu and Yb and trivalent Tb. Some terbium-iron intermetallic compounds and, in particular, the Laves phase $TbFe_2$, possess exceptionally interesting properties such as giant magnetostriction[8,9] and huge ΔE effect.[10] These compounds are therefore considered as being potentially useful materials for various applications. In order to facilitate the development of technologically useful materials based on these compounds, we undertook the determination of the Tb-Fe phase diagram by means of standard metallographic, DTA, X-ray diffraction, and electron microprobe analysis techniques.

The presence of four intermetallic compounds, namely $TbFe_2$, $TbFe_3$, Tb_6Fe_{23}, and Tb_2Fe_{17} has been previously reported.[11] There is lack of agreement, however, concerning the existence of the Tb_6Fe_{23} compound. Kripyakevich et al.[12] and Ray[11] report its presence; whereas, according to Oesterreicher,[13] Tb_6Fe_{23} was not found either in cast or in heat-treated alloys. Only by substituting some Al for Fe could it be prepared.[13] On the other hand, it proved practically impossible to prevent the formation of Tb_6Fe_{23} in alloys prepared by powder metallurgical techniques.[14] Contradictory reports have also been given concerning the structure-type of the Tb_2Fe_{17} compound.[13,15] In the course of the present study efforts were made to clarify these issues.

Experimental Techniques

Alloy Preparation and Metallography

The alloys were prepared by arc melting 99.99% pure iron and 99.9% pure terbium (Research Chemicals, Phoenix, Arizona), on a water-cooled copper hearth under a zirconium gettered argon atmosphere. Each alloy button, weighing 5-10 grams was turned over and remelted several times in order to ensure a good homogeneity.

For heat treatments up to 1100°C, the samples were wrapped in thin tantalum foils and sealed in evacuated quartz capsules. For higher temperature anneals, the quartz capsules were back-filled with a partial pressure of argon.

The metallographic preparation of the samples consisted in standard cold mounting, grinding and polishing techniques. The final polishing stage consisted of vibratory polishing with a Linde γ alumina water suspension. A 1% nital solution was used for etching the polished samples. A 3% ferric chloride solution was useful for revealing the grain structure of iron-rich compounds. Essentially, a similar, though particularly careful procedure was followed in order to reveal magnetic domain patterns detectable by the Kerr effect.

Thermal Analysis

The differential thermal analysis (DTA) runs were carried out on 5-7 gram samples in tantalum crucibles for rare-earth-rich alloys. Boron nitride or recrystallized alumina crucibles were used for the iron-rich samples. The temperatures were measured with suitably sheathed Pt-Pt 10 Rh thermocouples. A protective argon atmosphere was used. The argon in a closed circuit was purified by passing it over Ti chips at 850°C and through a liquid nitrogen trap.

X-Ray Diffraction and Electron Microprobe Analysis

For X-ray analysis a Pickart diffractometer was employed using Cu K_α

radiation in conjunction with an X-ray monochromator. The diffraction patterns were indexed with the help of an X-ray powder diffraction pattern generating computer program. Lattice parameters were determined using Cohen's least-squares fit method. In several instances a MAC (Materials Analysis Company) electron microprobe was used for phase identification and for checking the terminal solubility of terbium in iron. Unfortunately, the relative closeness of the relevant Tb lines, Tb L_{α_1}, and Tb L_{β_1} to the Fe lines K_α and K_β, respectively, detracted from the accuracy of the solubility determinations.

Results and Discussion

On the basis of the DTA thermal arrests and the information provided by the X-ray and micrographic analyses, the phase diagram shown in Fig. 1 was constructed. The invariant temperatures of the eutectic and of the four peritectic reactions were determined from the thermal arrests appearing on the heating curves. The possible error for the eutectic temperature is ±3°C; for the peritectics, ±5°C.

Terminal Solid Solubilities

The solubility of iron in terbium is below the detection limit of the experimental techniques employed in this study. The addition of iron to terbium does not affect the temperature of the α(HCP) to β(BCC) transformation in terbium (1318±2°C). From radioactive tracer diffusion studies,[16] it has been recently inferred that a significant fraction of dissolved iron in the light rare-earth metals, Ce, Pr, and Nd is located on interstitial sites. It would be interesting to check in what way does the lanthanide contraction in the heavier rare-earth metals like terbium, affect that tendency.

The results of the DTA runs indicated that the temperature of the $\alpha \rightarrow \gamma$ phase transformation in iron is slightly increased, while that of the $\gamma \rightarrow \delta$ transition is decreased by terbium additions. This behavior is similar to that observed in all other rare-earth iron systems, with the exception of Er, for which there is conflicting evidence.[5-6] The rare-earth metals, including terbium, act, therefore, as BCC stabilizers, with a severely limited solubility. The lattice parameter of a Tb saturated solid solution, quenched from 880°C is slightly increased to 2.8672±0.0002 Å, as compared to its value (2.8664 Å) in pure iron. Assuming a linear dependence of the lattice parameter on Tb concentration (Vegard's Law), the solubility limit would be 0.07±0.03 at.%. Using electron microprobe measurements, a value of 0.1±0.05 at.% Tb was found, roughly agreeing with the lattice parameter measurements. No significant difference was observed for Tb-saturated solid solutions quenched from the γ temperature interval.

The Intermetallic Compounds

Similar to all other rare-earth iron binary systems from Gd onto Lu (with the exception of unknown Yb), four intermetallic compounds are present in the Tb-Fe system. Structural data concerning these compounds is given in Table I.

$TbFe_2$ and $TbFe_3$

The eutectic temperature between Tb and the first iron-containing compound, $TbFe_2$, is situated at 28±0.5 at.% Fe and 847±3°C. The microstructure of a slowly (5°/min) cooled hypereutectic alloy (Fig. 2) reveals primary $TbFe_2$ dendrites, embedded in a Tb-$TbFe_2$ eutectic matrix. Dwight and Kimball[17] have recently shown that the $TbFe_2$ compound is a rhombohedrally-distorted Laves phase. The rhombohedral distortion although small ($\alpha = 59.6°$, instead of 60° for a regular cubic C-15 structure) is clearly apparent when checking the medium and high angle diffraction line profiles. The rhombohedral distortion is a direct result of the giant [111]-type magnetostriction present at room temperature in $TbFe_2$.

The Laves phase $TbFe_2$ melts non-congruently at 1187°C. In this respect it is interesting to note that with increasing atomic number of the rare earth component, (R), the ratio of the atomic radii components r_R/r_{Fe} gets closer to the ideal Laves phase ratio, 1.225. This is reflected by the increasing stability of the RFe_2 phases. Thus, from $SmFe_2$ to $HoFe_2$, these compounds melt non-congruently at increasingly higher temperatures. From $ErFe_2$ to $LuFe_2$ they melt congruently at temperatures above 1300°C. A similar trend is, by the way, also observed in the RCo_2 series.

The minority phase, in the two-phase $TbFe_2$-$TbFe_3$ region, appears in the form of elongated platelets (Fig. 3). Slowly cooled alloys in this two-phase region revealed the presence of a precipitation reaction taking place within the $TbFe_2$ grains. In rapidly quenched samples no such precipitation could be detected. A definite orientation relationship is apparent between the iron-rich thin platelets, forming 120° angles among themselves, and the parent grains. The microstructure of a sample annealed for 2 hr at 1100°C, followed by an 8 hr long anneal at 700°C, is shown in Fig. 4. A phase boundary between a $TbFe_3$ on the left side and a $TbFe_2$ grain on the right, runs along the figure. Noteworthy is that no precipitation occurred in the $TbFe_2$ grain, in regions adjacent to the grain boundary, presumably because the excess iron, instead of precipitating, diffused during the low-temperature anneal towards the phase boundary. It follows that, similar to the Er-Fe system as observed by Meyer,[5] $TbFe_2$ has a homogeneity range at elevated temperatures extending towards iron-rich compositions. This composition interval is schematically shown by dashed lines in Fig. 1. Efforts were made to confirm such a homogeneity range by comparing lattice parameters of alloys having compositions which bracket that of $TbFe_2$. No difference, within experimental errors, was observed. The experimental errors on the lattice parameters of the rhombohedrally-distorted compounds are, however, much larger than for an ordinary cubic Laves phase. Similar lattice parameter measurements on both sides of the stoichiometric $TbFe_3$ composition did not confirm Gilmore and Wang's[18] reported homogeneity range for this compound.

Tb_6Fe_{23}

The X-ray patterns of arc-melted samples of composition ranging from 75-90 at.% Fe contained only the diffraction lines corresponding to the $TbFe_3$ and Tb_2Fe_{17} phases. A lengthy anneal of 14 D at 1220°C of a 79.5 at.% Fe sample yielded, however, a nearly single phase Tb_6Fe_{23} structure. The melting point of this compound, as shown by the thermal arrest on its heating curve, is situated at 1276°C. Noteworthy is that this sample did not contain any detectable Tb_6Fe_{23} phase upon relatively rapid (20°/min.) cooling subsequent to its melting. It again required a lengthy high-temperature anneal in order to cause the reappearance of $TbFe_{23}$. Similar difficulty in the nucleation of this phase has been observed in the Dy-Fe[2] and Gd-Fe[2] systems. Earlier published phase diagrams of this latter system[19] fail to make mention of the presence of Gd_6Fe_{23}. The lengthy anneals required at relatively elevated temperatures (>1100°C) would account for the recent report that this phase is absent in the Tb-Fe system.[13] In agreement with Oesterreicher's findings,[13] we also observed that ternary additions, oxygen in our case, greatly enhance the rate of nucleation and growth of the Tb_6Fe_{23} phase. Very slow cooling at 1°/min through the 1400-1200°C temperature interval yielded a microstructure which did clearly show the peritectic nature of the compound formation, as shown in Fig. 5. The lattice parameters of Tb_6Fe_{23} are in good agreement with those previously reported by Ray.[11]

Tb_2Fe_{17}

Contrary to the previous compound, Tb_2Fe_{17} single phase samples were easily obtained, even though both compounds melt non-congruently. This is illustrated in Fig. 6, for a 92 at.% Fe sample showing primary Fe dendrites surrounded by the Tb_2Fe_{17} matrix. Figure 7 shows the highly twinned microstructure of a 89.5 At.% Fe sample, corresponding to the stoichiometric Tb_2Fe_{17} composition.

Alloys of the rare-earth metals with approximately 89 at.% of transition metals Fe, Co, or Ni have been reported to possess either a hexagonal Th_2Ni_{17} or a rhombohedral Th_2Zn_{17}-type structure. Both structure types may be regarded as different stacking sequences of a basic structural layer related to the $CaCu_5$-type structure. The occurrence of these various structure types has been discussed by Buschow[15] and by Givord <u>et al</u>.[20] It appears that with decreasing rare-earth size, the $ThNi_{17}$-type structure is favored. Thus, one finds the Th_2Zn_{17}-type for the light rare-earth elements Ce to Gd, while the Th_2Ni_{17}-type is present in Dy to Er-iron systems. The atomic size of Tb places it at the borderline between these two groups.

According to Buschow,[15] the common room temperature modification of $TbFe_{17}$ is the Th_2Zn_{17} structure type. The Th_2Ni_{17} type could be found only in splat cooled samples. Oesterreicher[13] on the other hand, observed only the Th_2Ni_{17} type structure, both for the as cast and for samples given a prolonged anneal at relatively low (700 and 880°C) temperature.

Our results indicate that both the Th_2Zn_{17} and the Th_2Ni_{17} structure types are present in the Tb-Fe system. The rhombohedral Th_2Zn_{17} type was found in all samples having a composition on the Tb-rich side of the Tb_2Fe_{17} composition, while the Th_2Ni_{17} type was found on the iron-rich side. We believe that the strongly twinned structure shown in Fig. 7 represents a mixture of the two structure types. The hexagonal structure type was always and exclusively observed in iron-rich Tb_2Fe_{17} samples, irrespective of the annealing temperature (1200°C, 8 hr; 1000°C, 24 hr; 800°C, 72 hr). On the other hand, rapidly cooled Tb-rich samples yielded a mixture of the Th_2Zn_{17} and Th_2Ni_{17} structure types. A two hour anneal at 1200°C was sufficient, however, to result in a purely rhombohedral Th_2Zn_{17} type structure.

These findings seem in qualitative agreement with Givord et al. analysis of the 2:17 compounds. Both the Th_2Zn_{17} and the Th_2Ni_{17} variants are derived from the $CaCu_5$ type structure by orderly substitution of a pair of transition metal atoms for each third rare-earth atom. The Th_2Ni_{17} hexagonal variant retains, however, some disorderly substitutions and is, therefore, more able to accommodate excess transition metal atoms and also tends to be more stable at elevated temperatures. Whether the two structure variants at room temperature are equilibrium structures having slightly different compositions, implying thereby a finite width in the region corresponding to the 2:17 phase, has not been ascertained in the present study.

Finally, we wish to mention that careful sample surface preparation reveals the magnetic domain pattern by use of the Kerr effect. In Fig. 8 the different domain width in three different terbium-iron intermetallic compounds is shown. This technique offers, potentially, a highly useful tool for studying some aspects of the exceptional magnetic anisotropy properties of the these compounds.

Acknowledgment:

We wish to thank G. Gordon, Jr., J. Jacobsen, and M. Malekzadeh for their helpful cooperation.

This work was supported by the U. S. Energy Research and Development Administration.

References

1. K. H. J. Buschow, J. Less-Common Metals 25 (1971) 131.

2. E. M. Sivitsky, V. F. Terekhova, R. S. Torchinova, I. A. Markova, O. P. Naumkin, V. E. Kolesnichenko and V. F. Stroganova, Les Elements des Terres Rares, p. 47. Editions du Centre National de la Rechercho Scientifique, Paris (1970).

3. A. S. Van der Goot and K. J. Buschow, J. Less-Common Metals, 21 (1970) 151.

4. G. J. Roe and T. J. O'Keefe, Met. Trans., 1 (1970) 2565.

5. A. Meyer, J. Less-Common Metals, 18 (1969) 41.

6. K. H. J. Buschow and A. S. Van der Goot, Phys. Stats. Solidi, 35 (1969) 515.

7. V. E. Kolesnichenko, V. F. Terekhova, and E. M. Savitskii, Metalloved. Isvet. Metal. Splavov 1972, Edited by M. E. Drits, "Nauka" Moscow, U.S.S.R.

8. N. Koon, A. Schindler, and F. Carter, Phys. Letts. 37A (1971) 413.

9. A. E. Clark and H. S. Belson, Phys. Rev., B5 (1972) 3642.

10. H. Klimker, M. Rosen, M. P. Dariel, and V. Atzmony, Phys. Rev., B10 (1974) 2968.

11. A. E. Ray, Proc. 7th Rare Earth Res. Conf., Coronado, Calif. (1968) p. 473.

12. P. I. Kripyakevich and D. P. Frankevich, Sov. Phys. Crystallography, 10 (1966) 468.

13. H. Oesterreicher, J. Less-Common Metals, 40 (1975) 207.

14. M. Malekzadeh, M. D. Dariel, and M. R. Pickus, to be published.

15. K. H. J. Buschow, J. Less-Common Metals, 11 (1966) 204.

16. M. D. Dariel, Acta Met. 23 (1975) 473.

17. A. E. Dwight and C. W. Kimball, Acta Cryst., B30 (1974) 2791.

18. G. M. Gilmore and F. E. Wang, Acta Cryst., 23 (1967) 177.

19. R. P. Elliott, "Constitution of Binary Alloys, First Supplement" McGraw-Hill, New York, N.Y., 1965, p. 414.

20. D. Givord, F. Givord, R. Lemaire, W. J. James, and J. S. Shan, J. Less-Common Metals, 29 (1972) 389.

TABLE I

Structural Data for the Tb-Fe Intermetallic Compounds

Compound	Crystal Symmetry	Space Group	Structure Type	Lattice Parameters (Å)
$TbFe_2$ (room temperature)	Rhombohedral	$\underline{R\bar{3}m}$	Distorted $MgCu_2$	a = 5.1896 [a] c = 12.8214 (hex. axes)
$TbFe_3$	Rhombohedral	$\underline{R\bar{3}m}$	$PuNi_3$	a = 5.139±0.001 c = 24.610±0.002 (hex. axes)
Tb_6Fe_{23}	Cubic	$\underline{Fm3m}$	Th_6Mn_{23}	12.085±0.002
Tb_2Fe_{17} (Tb-rich side)	Rhombohedral	$\underline{R\bar{3}m}$	Th_2Zn_{17}	a = 8.504±0.004 c = 12.413±0.002 (hex. axes)
Tb_2Fe_{17} (Fe-rich side)	Hexagonal	$\underline{P6_3/mmc}$	Th_2Ni_{17}	a = 8.472±0.004 c = 8.321±0.002

[a] Results taken from Ref. 17.

Figure Captions

Fig. 1. The Terbium-iron phase diagram.

Fig. 2. Hypereutectic 52. at.% Fe alloy. Primary $TbFe_2$ dendrites in a $Tb-TbFe_2$ eutectic matrix (x400).

Fig. 3. Primary elongated $TbFe_3$ platelets in a $TbFe_2$ matrix of a 68 at.% Fe alloy phase contrast at (x600).

Fig. 4. 68 at.% alloy, annealed for 2 hr at 1100°C and subsequently for 8 hr at 700°C. The $TbFe_3$ grain lies on the left, $TbFe_2$ on the right. Iron-rich plate-like precipitates are present in the $TbFe_2$ grain. Note their absence in the region adjacent to the phase boundary (x400).

Fig. 5. 79.5 at.% Fe alloy slowly (1°/min) cooled through the 1400-1200°C temperature range. Grain "a" is primary Tb_2Fe_{17}, surrounded by peritectically formed Tb_6Fe_{23} (grains "e"). Final product of solidification $TbFe_3$ (grain "i") (x1000).

Fig. 6. 92 at.% Fe alloy. Primary Fe dendrites embedded in a Tb_2Fe_{17} matrix (x100).

Fig. 7. Strongly twinned 89.5 at.% Fe sample, believed to represent a mixture of the two, Th_2Zn_{17} and Th_2Ni_{17} type structure variants of Tb_2Fe_{17} (x400).

Fig. 8. Magnetic domain pattern of the same area as in Fig. 5, revealed through the Kerr effect, illustrating the different domain width in three different Tb-Fe intermetallic compounds. The arrow points to an area where reverse magnetization domain spikes appear (x1000).

0 0 0 0 4 3 0 5 5 6 5

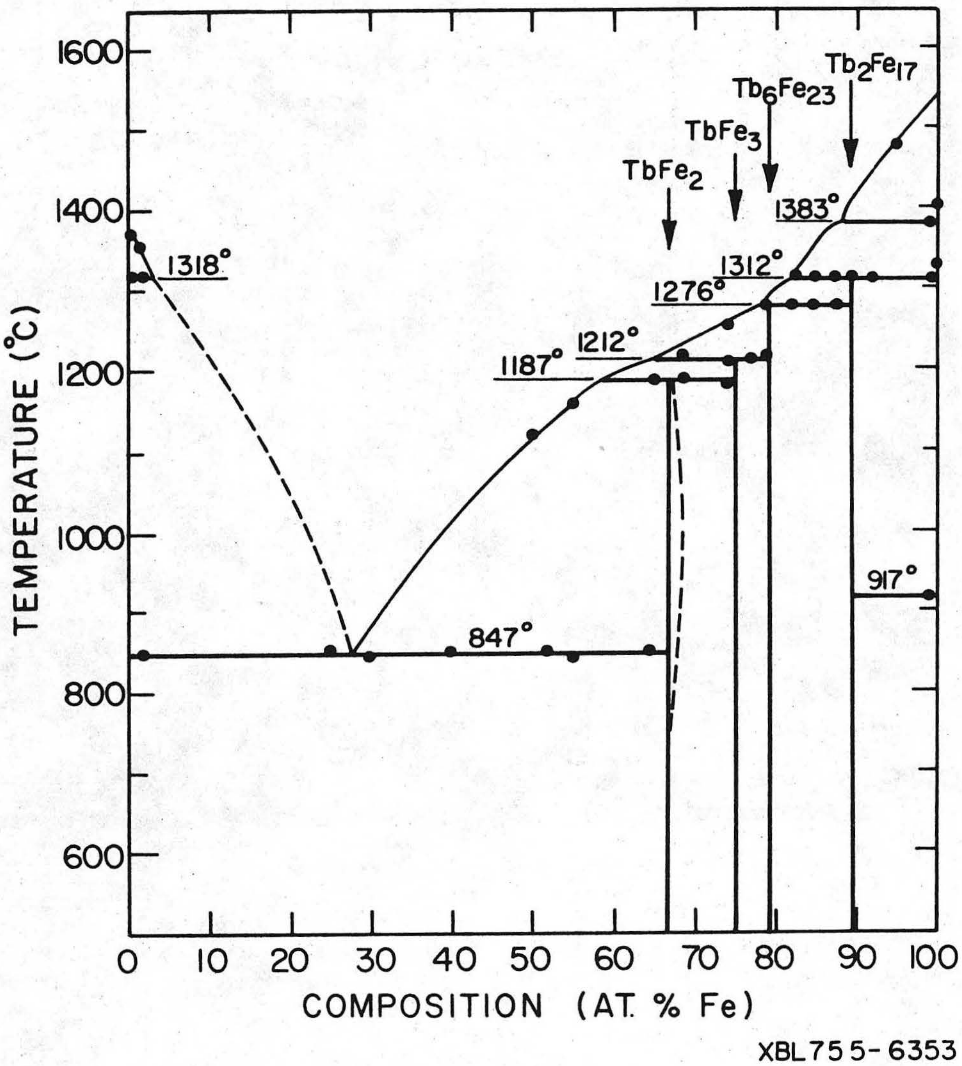

Fig. 1

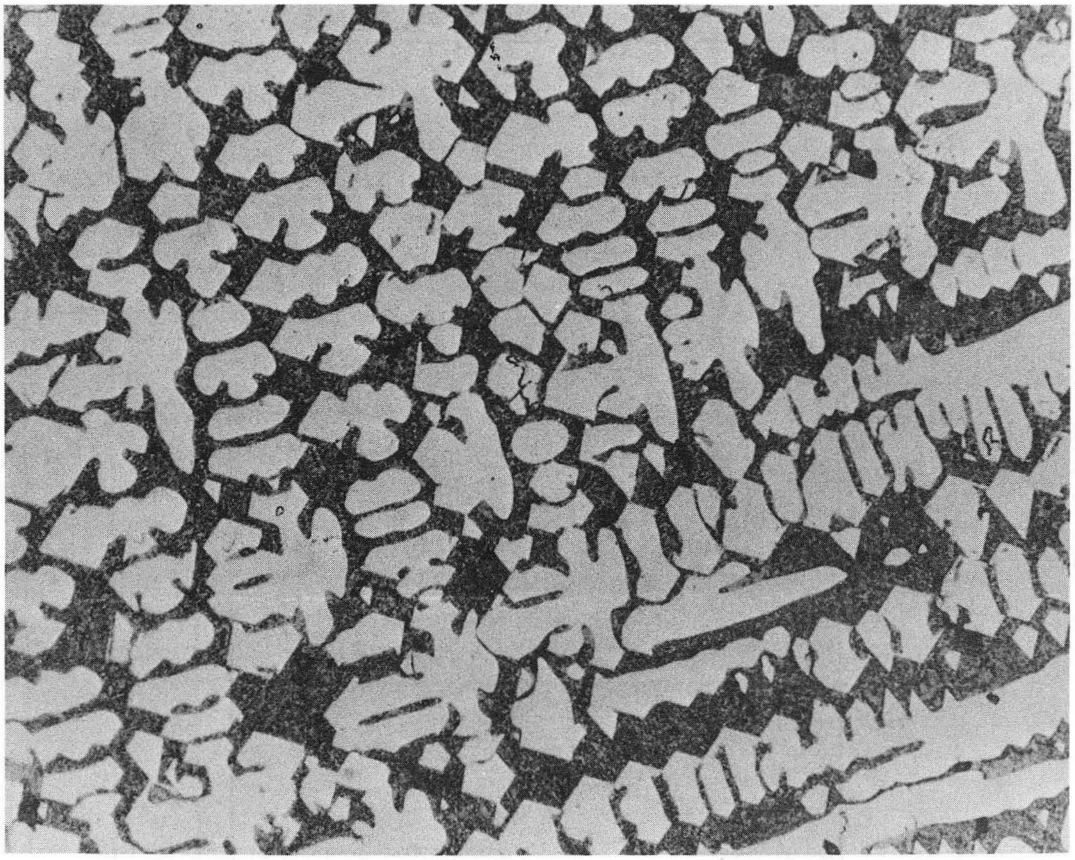

XBB 755-3917

Fig. 2

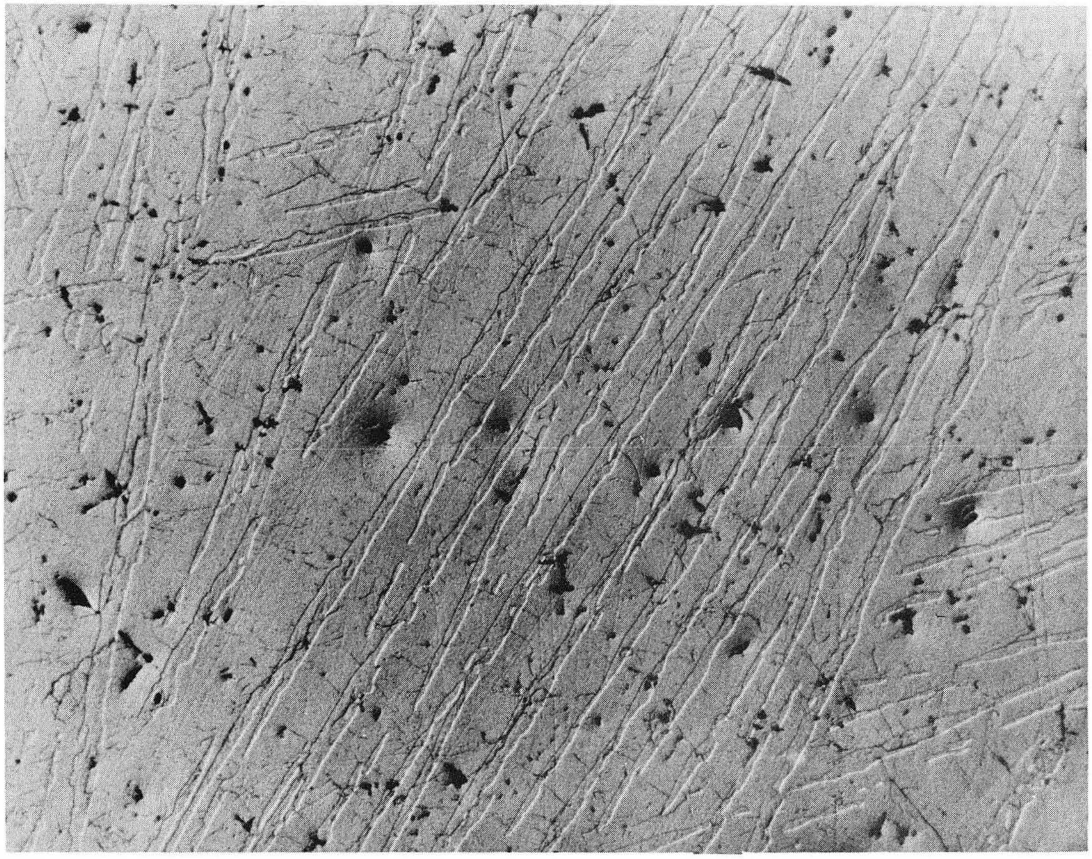

XBB 755-3921

Fig. 3

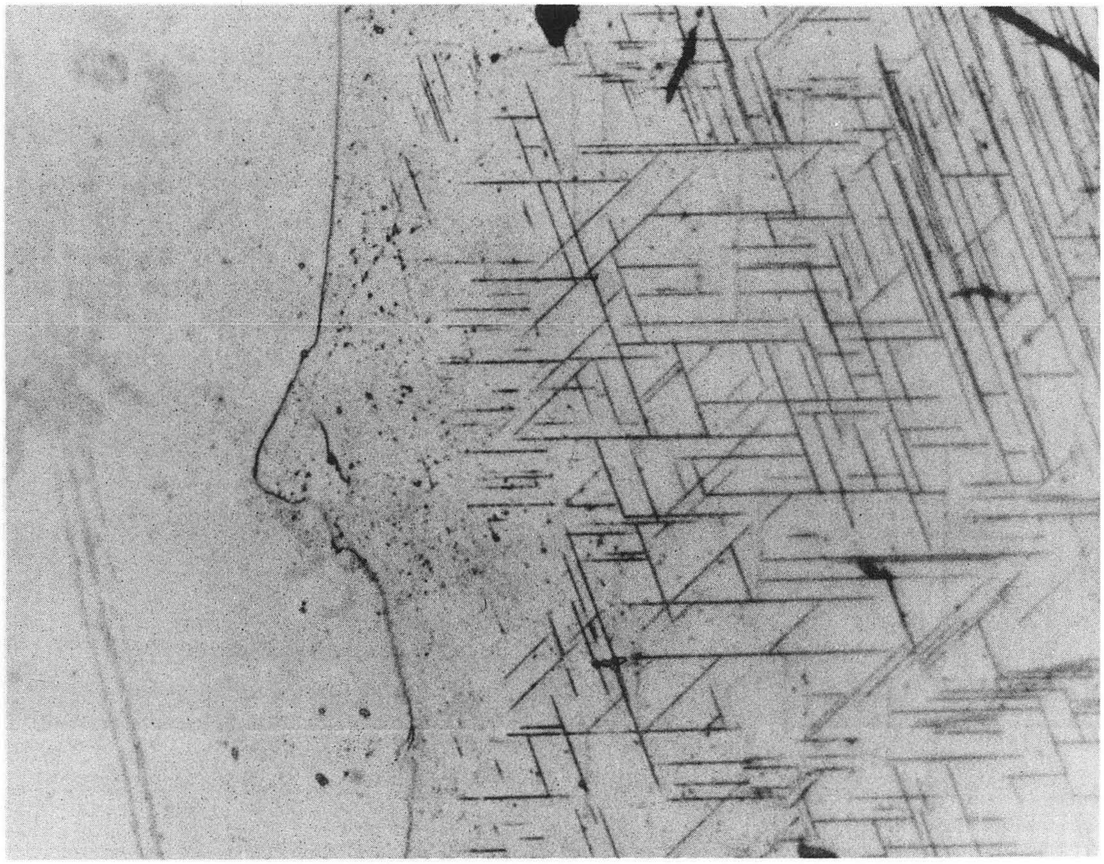

XBB 755-3922

Fig. 4

0 0 0 0 4 3 0 5 5 6 7

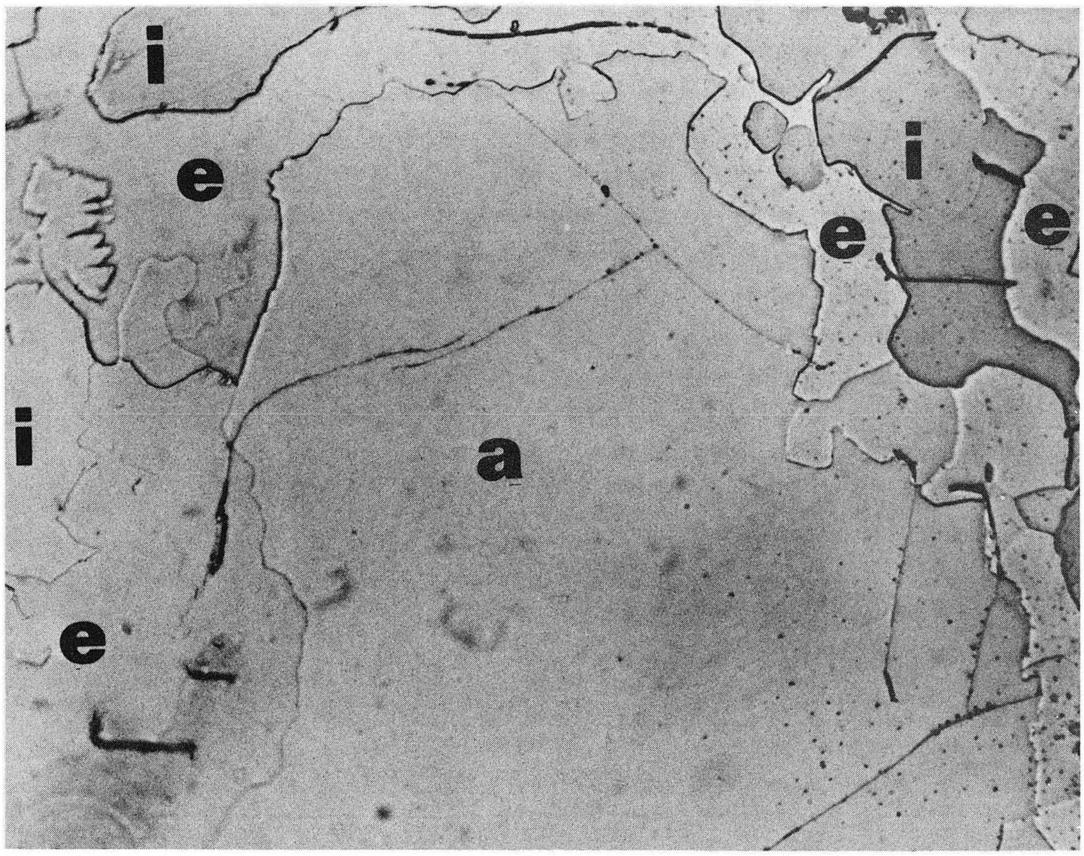

XBB 755-3916

Fig. 5

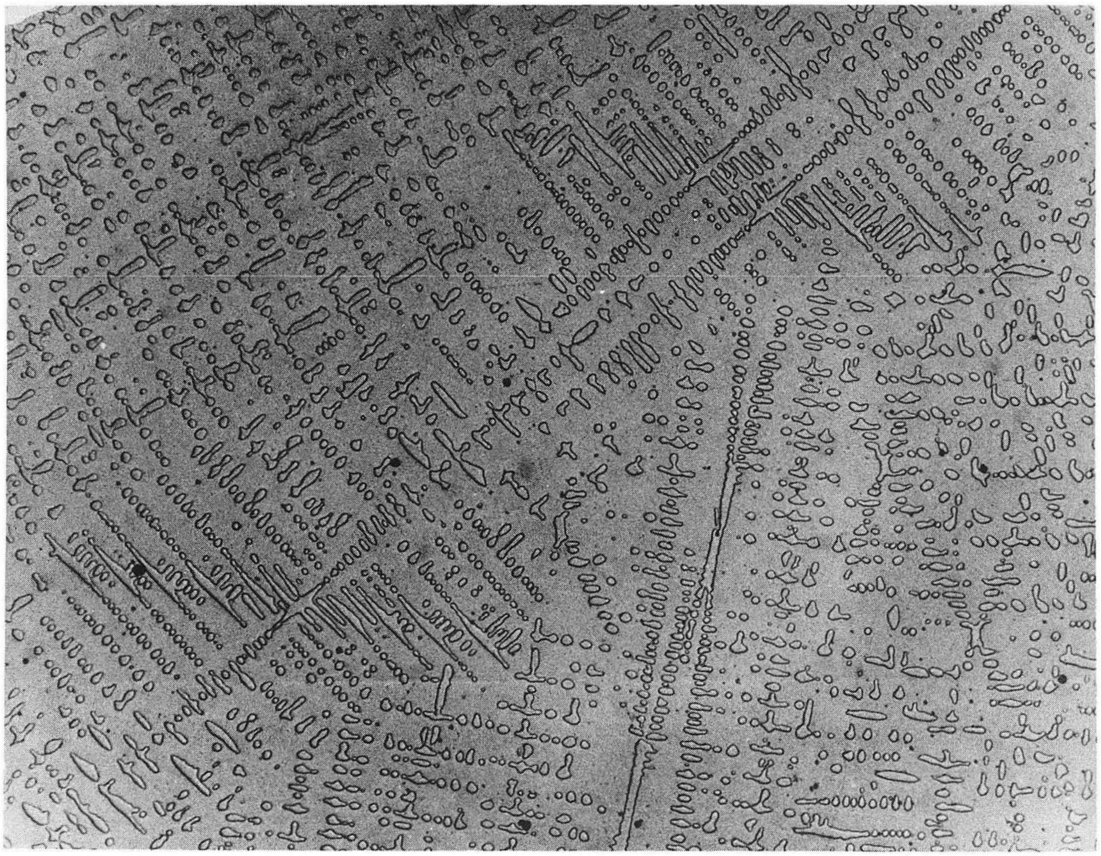

XBB 755-3920

Fig. 6

0 0 0 0 4 3 0 5 5 6 8

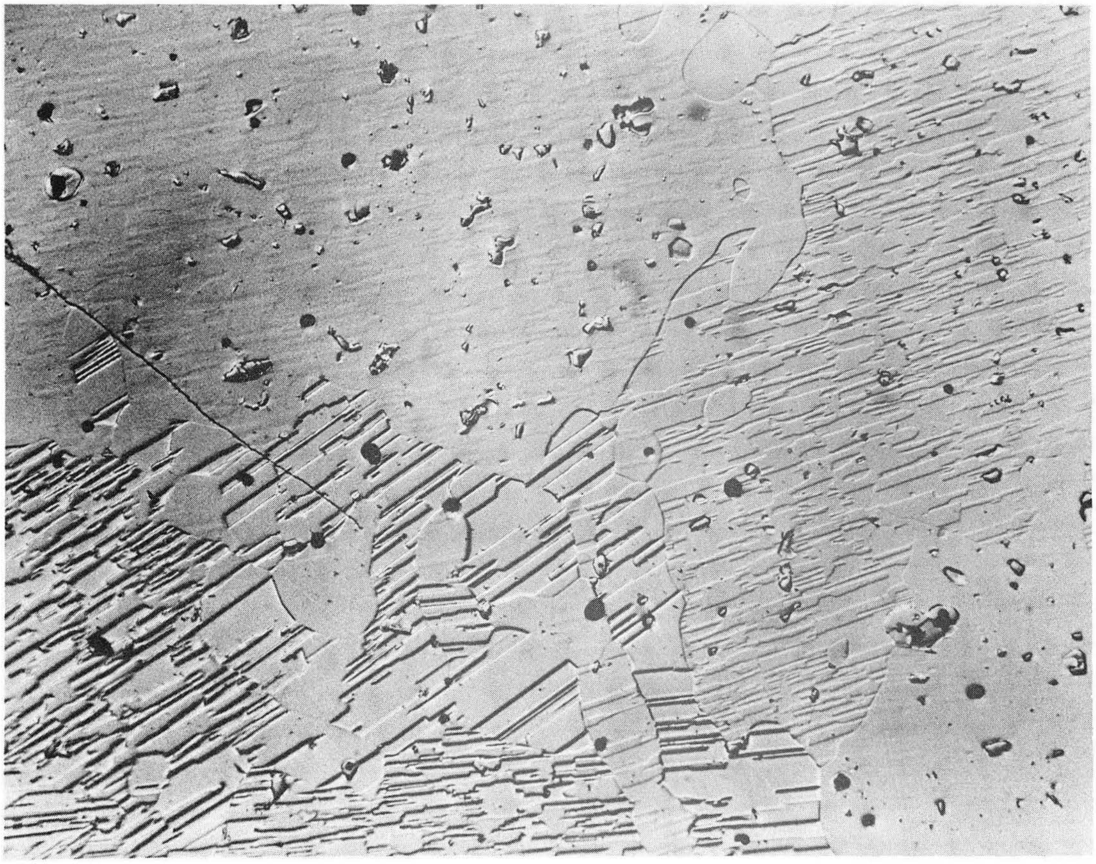

XBB 755-3919

Fig. 7

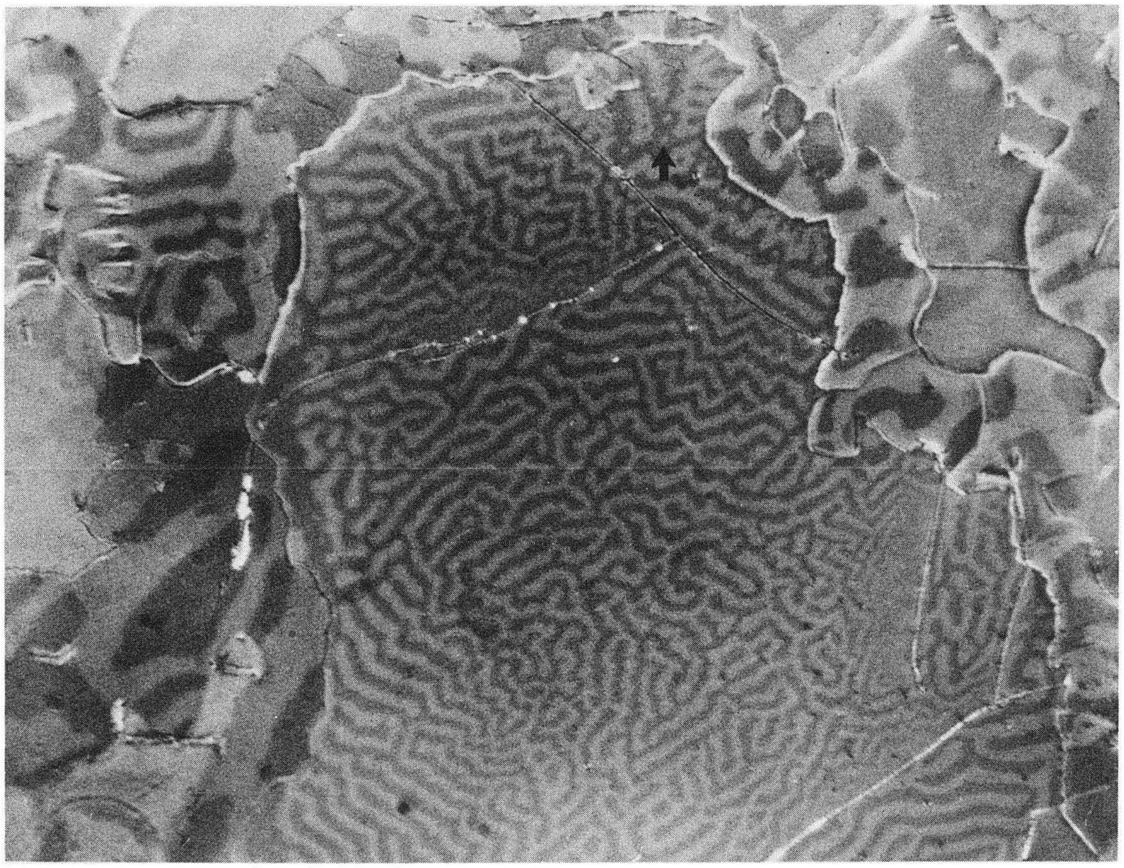

XBB 755-3918

Fig. 8

0 0 0 0 4 3 0 5 5 6 9

LEGAL NOTICE

This report was prepared as an account of work sponsored by the United States Government. Neither the United States nor the United States Energy Research and Development Administration, nor any of their employees, nor any of their contractors, subcontractors, or their employees, makes any warranty, express or implied, or assumes any legal liability or responsibility for the accuracy, completeness or usefulness of any information, apparatus, product or process disclosed, or represents that its use would not infringe privately owned rights.

TECHNICAL INFORMATION DIVISION
LAWRENCE BERKELEY LABORATORY
UNIVERSITY OF CALIFORNIA
BERKELEY, CALIFORNIA 94720